Mixing of Non-Newtonian Fluids in Steadily Forced Systems

Paulo E. Arratia,* Troy Shinbrot, Mario M. Alvarez, and Fernando J. Muzzio

Department of Chemical & Biochemical Engineering, 98 Brett Road, Rutgers University, Piscataway, NJ 08855, USA

(Received 28 September 2004; revised manuscript received 28 September 2004; published 28 February 2005)

We investigate mixing in a viscoelastic and shear-thinning fluid—a very common combination in polymers and suspensions. We find that competition between elastic and viscous forces generates self-similar mixing, lobe transport, and other characteristics of chaos. The mechanism by which chaos is produced is evaluated both in experiments and in a simple model. We find that chaotic flow is generated by spontaneous oscillations, the magnitude and frequency of which govern the extent of chaos and mixing.

DOI: 10.1103/PhysRevLett.94.084501 PACS numbers: 47.52.+j, 47.15.–Gf, 47.50.+d, 83.50.Xa

Fluid mixing is an important process in many industries, nature, and everyday life. The discovery that simple, nonturbulent velocity fields can evolve into complicated motions through chaotic advection [1] has generated a great deal of interest in fluid mixing [2–6]. Previous research has been mainly restricted to Newtonian fluids, often in idealized model flows [2,5,6]. Most practical viscous fluids, by contrast, contain polymers or solids (e.g., pastes and colloids) and are not Newtonian. Such fluids are extremely common in both industry (e.g., cell fermentation and polymer processing) and nature (e.g., lava and synovial fluid). An important feature of many non-Newtonian fluids is that they often exhibit both viscoelasticity and shear-thinning viscosity.

Most mixing investigations have considered only ''ideal'' constitutive behavior (i.e., either elastic or shear-thinning). Fluids that are viscoelastic but not shear-thinning (''Boger fluids'') [7], are often used to investigate the effects of viscoleasticity on mixing [8,9] and fluid instabilities [10–12] at low Reynolds numbers (Re). For example, Groisman and Steinberg [13] showed an increased resistance to forcing, irregular flow patterns, and other complex features at negligible inertial stresses in a simple flow. These effects appear when the elasticity number, $El = Wi/\mathrm{Re}$, is large (>1), where Wi (Weissenberg number) is the product of the characteristic rate of deformation ($\dot{\gamma}$) and the longest fluid relaxation time (λ). These findings imply that viscoelastic effects may enhance mixing, as has also been shown in a curved channel [9]. By contrast, experimental and numerical studies of mixing of constant viscosity, elastic fluids in 2D time-periodic flows have shown that elasticity can *either* increase or decrease chaotic motion, apparently because the effect of elasticity on mixing depends on the mixing protocol [8,14–16]. In a similar geometry, a computational study found that shear-thinning viscosity without elasticity *decreases* both the rate and extent of mixing [17]. However, for non-Newtonian fluids that are both shear-thinning and viscoelastic, it is difficult to predict *a priori* how these effects will interact. The few available mixing investigations of shear-thinning viscoelastic fluids have focused either on macroscopic aspects of the flow [18,19] or have been of qualitative nature [20]. As a result, the mechanisms responsible for mixing of such fluids are not fully understood.

In this Letter, we report the onset of spontaneous chaos in a simple geometry, a tank stirred by a single axisymmetric disc in a fluid that is both shear-thinning and viscoelastic. We analyze the mixing mechanism in experiments and in a simple model. In Fig. 1, we display results of dye advection experiments using planar laser induced fluorescence. Here a laser sheet illuminates a plane within the tank that is injected with a blob (3 ml, approximately 1 inch from the disk tip) of a neutrally buoyant passive fluorescent tracer (Rhodamine G6). As the dye advects, areas illuminated correspond to intersections of the laser sheet with the dye. In Fig. 1(a), we show an illuminated slice through the axis of the mixing tank filled with a Newtonian fluid (glycerin, $\rho = 1.2\ \mathrm{g/cm^3}$, $\eta = 700$ cp) at $\mathrm{Re} = 10$, defined as $\mathrm{Re} = \rho N D^2/\eta$, where N is the impeller agitation speed in Hz, D is the impeller diameter (7.5 cm), ρ is the fluid density, and η is the fluid viscosity. The snapshot reveals closely spaced, concentric sets of rings surrounding elliptic points, demonstrating that fluid does not mix down to very small length scales. This is as expected: no signs of chaotic mixing are observed since at low Re every azimuthal slice through the system is identical and the flow is effectively steady, 2D and integrable (this remains the case up to $\mathrm{Re} = 190$). Mixing occurs only by slow diffusion and patterns remain unchanged on scales of hours.

Figure 1(b) reveals an entirely different behavior if we replace the Newtonian fluid with a 1%-aqueous carboxymethyl cellulose (CMC, 2.7×10^6 MW) solution which is both shear-thinning and viscoelastic [21] at $\mathrm{Re} = 13.5$ and $Wi = 2.75$. A lobe formation process is now observed. Lobe structures, identified by the green line in Fig. 1(b), indicate that the ingredients of chaotic mixing—folding and stretching—are present. In addition, two distinct flow regimes are observed: a ''high-shear'' region identified by the red line in Fig. 1(b), located around the disk, and an ''elastic'' region that spreads throughout the rest of the tank. The former region is characterized by Newtonian-like flow patterns, where fluid motion is proportional to applied

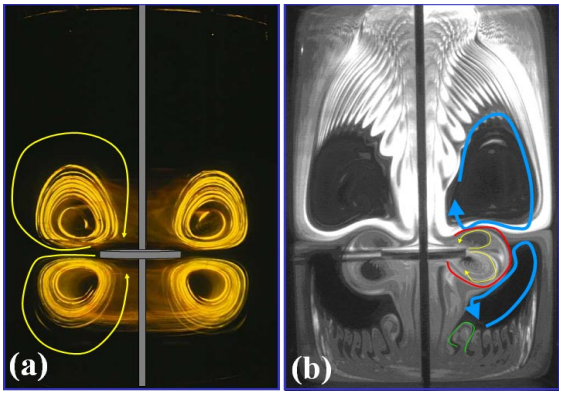

FIG. 1 (color online). Flow patterns of a tank ($D_T = 24$ cm and $H = 32$ cm) stirred by an axysymmetric disc. (a) Newtonian fluid (glycerin) at Re = 10 reveals concentric rings and no signs of chaos. (b) Lobe formation and chaotic motion in a 1%-aqueous solution of CMC ($\lambda = 0.55$ s) at Re = 13.5 ($Wi = 2.75$). Shear rate dependent viscosity data are fitted to $\eta = \eta_0[1 + (\kappa\dot{\gamma})^2]^{-n/2}$, where $\eta_o = 3000$ cP is the zero-shear-rate viscosity, $n = 0.7$ is the power law index, and $\kappa = 1.2$ is a time constant. Yellow and blue lines show flow direction. Red line delimits the high-shear region. Green line contours a single lobe.

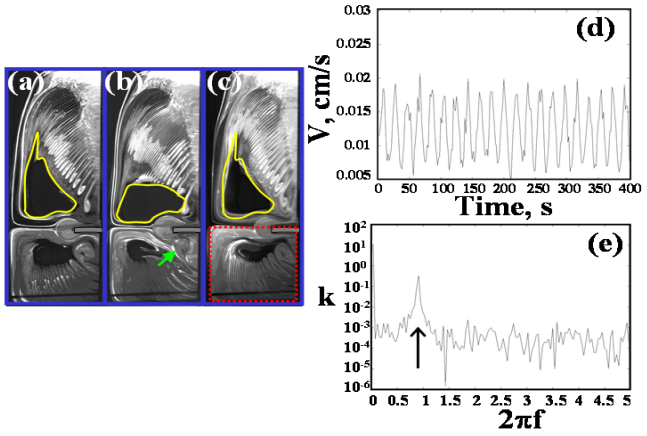

FIG. 2 (color online). Periodic flow oscillations of a shear-thinning elastic fluid (Re = 13.5, $Wi = 2.75$): snapshots of the mixing structure of 1% CMC 10 s apart. (a) initial, (b) $\Delta t = 10$ s, (c) $\Delta t = 20$ s. Yellow line identifies the upper segregated region. Green arrow (b) points to the region where lobes are created. Dashed red square (c) delimits area of interest for modeling. Periodicity of velocity field is also revealed via PIV (d) and power spectra (e) (arrow points to well-defined peak).

stress. Fluid in this region is expelled radially from the disk toward the tank walls (yellow arrows). Surrounding this inertial region is an elastic region where flow is *reversed*. Flow here convects dye vertically away from the disc (blue arrow) and recirculates it along the tank walls and then radially inward toward the disk again. Thus the mixing mechanism here seems to rely on an interaction between these two regions with opposite flow directions.

We can understand the regions of flow reversal for shear-thinning viscoelastic fluids in the following way: polymer molecules can stretch in curvilinear shear flows and often align themselves along the direction of the primary flow. The stretching of polymer molecules along streamlines leads to a normal stress difference $N1 \equiv \tau_{\theta\theta} - \tau_{rr}$, where r, θ, and z are cylindrical coordinates. This normal stress difference $N1 = -2\eta^p(\dot{\gamma})\lambda(\dot{\gamma})\dot{\gamma}^2$ produces a volume force $N1/r$ acting inward in the radial direction causing flow reversal. Here, we are assuming an Oldroyd-B model modified to account for shear-thinning viscosity, where η^p is the polymer viscosity defined as $\eta^p = \eta - \eta^s$ and η^s is the solvent viscosity [12,22]. This volume force, however, is counterbalanced by the pressure gradient $\partial p/\partial r$. Near the disc, where velocities are large, $\partial p/\partial r > N1/r$ and flow reversal is not observed. Far from the disc, in regions where $\partial p/\partial r < N1/r$, we observe flow reversal.

We can identify the mechanism by which lobes, and consequently chaotic mixing, arise by examining a series of dye advection experiments, as shown in Fig. 2(a)–2(c). The frames presented are consecutive snapshots of the evolution of the partially mixed structure. The time lapse between frames is about 10 s. The mixing structure here oscillates, as can be illustrated by tracking a region of the tank (upper segregated region—yellow lines) over time. By comparing frames (a) and (b), we find that the upper segregated region in frame (a) is larger and of different shape than in frame (b). As time evolves, the shape of the upper segregated region returns to its original state periodically, as shown in frame (c). However, the recurrent dyed structure incorporates more material on each successive period. Corresponding oscillating behavior appears in variations of the size and shape of the ''high-shear'' region. Close examination of fold structures reveals the advance of a train of folds originated at the join between disc and shaft [arrow in Fig. 2(b)]. Behavior in this small region, where the ''elastic'' and ''high-shear'' regions meet, seems to be central to the initiation of the lobes.

To quantify the time dependence of the flow (under steady forcing), we sample a small region between the tip of the disk and the tank wall, and average the magnitude of the velocity measured along a short path line using particle image velocimetry (PIV). Sampling times are long enough to ensure the accuracy of velocimetry measurement (1/4 s), but are shorter than the characteristic frequency of the fluid motion (close to 1 s). A representative sequence of velocity records and corresponding power spectrum for increasing agitation speeds is presented Fig. 2(d) and 2(e). These data show a well-defined periodic time dependence of the velocity in this flow at Re = 13.5 and $Wi = 2.75$. The peak in the power spectrum [arrow in Fig. 2(e)] is almost 4 orders of magnitude higher than background noise, confirming the appearance of Fig. 2(a)–2(c) that the flow is periodically perturbed.

We examine the effects of agitation speed on flow behavior at 150 RPM (Re = 5.63, $Wi = 1.38$), 300 RPM

(Re = 13.5, $Wi = 2.75$), 500 RPM (Re = 37.5, $Wi = 4.58$), and 750 RPM (Re = 84.38, $Wi = 6.88$). The basic flow structure remains unchanged in all four cases; flow reversal and lobe formation are invariably present (for $Wi < 0.9$, flow reversal is still observed, but there is no lobe formation, i.e., no mixing). However, the regular high-shear region grows as the agitation speed is increased. Mixing efficiency, which is assessed by recording the fractional area of the tank covered by the dye as a function of disc revolutions, therefore *worsens* as agitation speed is increased [Fig. 3(a)]. Area coverage is closely modeled as an exponential process, $A = A_{\max}(1 - e^{-KN})$, where $A_{\max}$ is the maximum area covered and K is the mixing rate. For all cases, coverage asymptotes at about 88%, but the rates are significantly different; 3.2×10^{-4}, 9.4×10^{-5}, 6.3×10^{-5}, and 5.7×10^{-5} rev^{-1} for 150, 300, 500, and 750 RPM, respectively. This result is counterintuitive insofar as the effects of elasticity would be expected *a priori* to be accentuated at higher shear rates and lower fluid viscosity.

The same trend is observed when quantifying the extent of chaotic mixing introduced by lobe formation in the system by the Melnikov method; single-lobe area may be considered as an effective measure of the degree of chaos in the system [23]. We therefore measure lobe areas from experimental snapshots by computing numbers of occupied pixels in digital images. We find that the lobe area (and hence the rate of chaotic mixing) decreases as frequency is increased. The cause of this effect appears to be that at high frequencies, lobes do not have enough time to fully stretch before folding, and so lobe sizes are small, which in turn hinders the mixing performance of the elastic region. At sufficiently low speeds, by contrast, lobes stretch more before folding, resulting in larger lobes that intrude further into the flow domain [Fig. 3(b)]. Since flow oscillation frequency (f) increases with agitation speed ($f = 4.3 \times 10^{-2} N^{1.48}$), [Fig. 3(b), inset], mixing efficiency is inversely related to agitation speed, in agreement with the mixing rate results. We speculate, but cannot confirm, that this flow oscillation may be directly linked to the longest fluid relaxation time (λ). This analysis is consistent with prior work that also reports oscillatory elastic instabilities in stressed viscoelastic fluids [10,12,20]. We believe that the instabilities observed in our experiments occur in regions where $\tau^p/\tau^s = \eta^p(\dot\gamma)\dot\gamma/\eta^s\dot\gamma > 1$, where $\tau^p = \tau - \tau^s = \eta^p(\dot\gamma)\dot\gamma$ is the elastic stress and $\tau^s = \eta^s\dot\gamma$ is the viscous stress. This threshold $[\eta^p(\dot\gamma)/\eta^s]$ is a function of radial position since $\dot\gamma$ varies in the radial direction due to the large gap between the outer wall and the disc. Hence, near the disc, where $\dot\gamma$ is high, the contribution of the polymer to the viscosity is small, and no instability is observed. As we move toward the tank wall, the elastic stresses (polymer molecules acting on the flow) start to increase as a power law and the region becomes susceptible to instabilities and oscillations.

To elucidate the mechanism by which lobes are formed and fluid is transported, we construct a map-based simulation intended to capture the iterative mapping described in Fig. 2. We focus our analysis on the right lower ''quadrant'' of the flow identified by the dashed red square in Fig. 2(c). The use of a periodic mapping is motivated by our experimental results, which indicate that the periodic oscillation of the ''high-shear'' region is correlated with the periodic formation of lobes. In short, flow visualization experiments show that when the ''high-shear'' region periodically contracts, fluid is drawn in and lobes are formed [green arrow in Fig. 2(b)], and as the high-shear region grows, the lobes are released downstream into the ''elastic'' region. The lobes are thereafter transported throughout this region and back into the ''high-shear'' region.

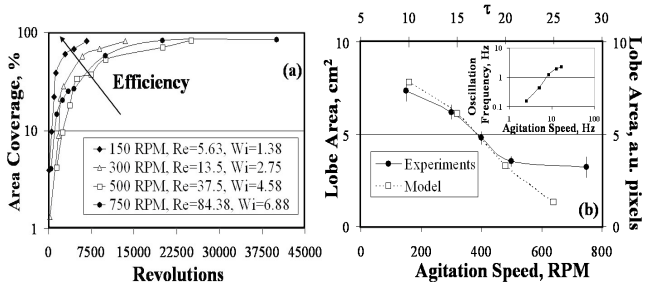

FIG. 3. Mixing efficiency worsens with agitation speed. (a) The rate by which a passive dye spreads is inversely related to agitation speed (Re and Wi). (b) Lobe-area measurements indicate that the extent of chaos decreases as frequency (agitation speed) is increased. Map results show that lobe area decreases with map frequency (τ). Insert: oscillation frequency increases with agitation speed.

Thus for our simulation, we construct a composite map to reproduce this behavior in a 2D square domain. The mapping consists of two parts: first, a circulatory flow mimicking the primary circulation within the red square of Fig. 2(c), and second, a periodic forcing that draws and expels material in the upper right quadrant of the square domain. Both parts of the mapping are area conserving. The circulatory flow is explicitly:

$$X_{n+1} = X_n - k_1{}^*\sin^2(Y_n) \tag{1}$$

$$Y_{n+1} = Y_n + k_1{}^*\sin^2(X_{n+1}), \tag{2}$$

where X_n and Y_n are Cartesian coordinates at time n, and k_1 defines the speed of the primary circulation [indicated by black arrows in Fig. 4(a)]. This map is supplemented by a secondary map defining periodic forcing only for points in the upper right quadrant [red dashed region in Fig. 4(a), where $x > 0$ and $y > 0$]:

$$u_{n+1} = u'_n + k_2{}^*\sin^2(v'_n) \tag{3}$$

$$v_{n+1} = v'_n - k_2{}^*\sin^2(u_{n+1}), \tag{4}$$

where $u' = u - k_2{}^*\sin^2(v)$ and $v' = v + k_2{}^*\sin^2(u')$. The secondary map has strength $k_2 = k_0[1 - \cos(2\pi^* n/\tau)]$, where k_0 is the perturbation strength and τ defines the frequency of the perturbation. If the strength of the sec-

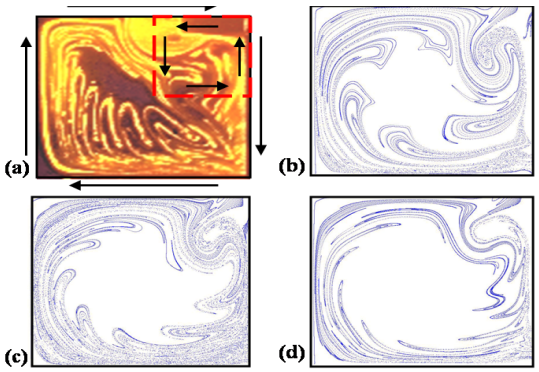

FIG. 4 (color online). (a) A 2D square lattice (black arrows) is periodically perturbed with a secondary map (red dashed lines) to mimic the experiments. The region of interest is the left lower quadrant of the tank [red dashed line on Fig. 2(c)]. Map is able to capture main features of the flow; compare (a) to (b). As frequency increases (τ), lobe area decreases and dye coverage diminishes for (b) $\tau = 15$, (c) $\tau = 20$, and (d) $\tau = 25$. Lobe area vs τ data is presented in Fig. 3(b).

ondary map is small ($k_0 < 1$), the "high-shear" region is comparatively weak, and we recover a nearly integrable flow with poor mixing.

This model faithfully captures the qualitative features of lobe formation [Fig. 4(b)], stretching, and transport seen in our experiment [cf. Fig. 4(a)]. In this simulation, we track an initial line of 5000 points for 300 iterations. In the context of this map, the mechanisms by which lobes are formed and transported can be understood by being dissected into two actions: an "inner" periodic circulation that is responsible for the *formation* of lobes and an "outer" circulation that is responsible for their *transport*. By increasing the inner map period (τ), we obtain larger folds, since folding frequency is reduced and stretching time is consequently prolonged [Fig. 4(b)–4(d)].

We interpret the results of this mapping as indicating that oscillations seen in our experiments may be produced at the interface between the two circulations observed, possibly through a competition between the principal relaxation time of the viscoelastic fluid (λ) and the forcing strain imposed by the rotating disks. The simplified map-based simulation also indicates, in agreement with previous observations [6,24], that the action of kinematic folding can be separated from the kinematics of gross material transport in low Re mixing systems. In other words, in systems such as the one considered in this Letter, mixing rates are not only a function of exponential stretching and folding, but are also dependent on transport throughout the vessel.

In conclusion, steady stirring of a shear-thinning and viscoelastic fluid produces the spontaneous emergence of chaos characterized by lobe formation and a stretching and folding engine that is driven by the interaction of a small inertial- and a large elastic-transport regions. We find that both the velocity field and flow structure are time dependent. The link between flow oscillations and the competition between fluid elasticity and imposed strain remain to be comprehensively investigated. The frequency of these oscillations is responsible for the mixing efficiency; high frequencies yield low quantitative extents of chaos and poor mixing efficiency. This is reproduced in a transport model in which a simple stretching and folding engine acts to generate iterated lobes.

*Current Address: Department of Physics, Haverford College, Haverford, PA 19041.

[1] H. Aref, J. Fluid Mech. **143**, 1 (1984).
[2] J. Chaiken, R. Chevray, M. Tabor *et al.*, Proc. R. Soc. London A **408**, 165 (1986).
[3] J. M. Ottino, *The Kinematics of Mixing: Stretching, Chaos, and Transport* (Cambridge University Press, Cambridge, England, 1989).
[4] F. J. Muzzio and P. D. Swanson, Phys. Fluids A **3**, 822 (1991).
[5] T. H. Solomon, S. Tomas, and J. L. Warner, Phys. Fluids **10**, 342 (1998).
[6] G. A. Voth, T. C. Saint, G. Dobler *et al.*, Phys. Fluids **15**, 2560 (2003).
[7] D. V. Boger, J. Non-Newt. Fluid Mech. **3**, 87 (1977).
[8] T. C. Niederkorn and J. M. Ottino, J. Fluid Mech. **256**, 243 (1993).
[9] A. Groisman and V. Steinberg, Nature (London) **410**, 905 (2001).
[10] R. G. Larson, E. S. G. Shaqfeh, and S. J. Muller, J. Fluid Mech. **218**, 573 (1990).
[11] E. S. G. Shaqfeh, Annu. Rev. Fluid Mech. **28**, 129 (1996).
[12] A. Groisman and V. Steinberg, Phys. Fluids **10**, 2451 (1998).
[13] A. Groisman and V. Steinberg, Nature (London) **405**, 53 (2000).
[14] C. W. Leong and J. M. Ottino, Phys. Rev. Lett. **64**, 874 (1990).
[15] S. Kumar and G. M. Homsy, Phys. Fluids **8**, 1774 (1996).
[16] Y. Fan, R. I. Tanner, and N. Phan-Thien, J. Fluid Mech. **412**, 197 (2000).
[17] T. C. Niederkorn and J. M. Ottino, AIChE J. **40**, 1782 (1994).
[18] A. B. Metzner and R. E. Otto, AIChE J. **3**, 3 (1957).
[19] A. W. Nienow and T. P. Elson, Chem. Eng. Res. Des. **66**, 5 (1988).
[20] J. R. Stokes and D. V. Boger, Phys. Fluids **12**, 1411 (2000).
[21] K. C. Tam and C. Tiu, J. Rheol. (N.Y.) **33**, 257 (1989).
[22] R. B. Bird, C. F. Curtiss, R. C. Armstrong *et al.*, *Dynamics of Polymeric Liquids: Fluid Mechanics* (Wiley, New York, 1987), Vol. 1.
[23] V. Rom-Kedar, A. Leonard, and S. Wiggins, Arch. Ration. Mech. Anal. **109**, 239 (1990).
[24] M. M. Alvarez, J. Zalc, T. Shinbrot *et al.*, AIChE J. **48**, 2135 (2002).